Spectroscopic investigation of the interaction of hydroxamate with bastnaesite (cerium) and rare earth oxides

Jianlan Cui [a], Gregory A. Hope [a,*], Alan N. Buckley [b]

[a] *Queensland Micro- and Nanotechnology Centre, School of Biomolecular and Physical Science, Griffith University, Nathan, QLD 4111, Australia*

[b] *School of Chemistry, The University of New South Wales, Sydney, NSW 2052, Australia*

* Corresponding author. Tel.: +61 7373 57550; fax: +61 7373 57773.

E-mail address: g.hope@griffith.edu.au

Address: Griffith University, Nathan, QLD, 4111, Australia

Abstract

Fourier transform infrared spectroscopy, Raman spectroscopy, X-ray photoelectron spectroscopy and scanning electron microscopy have been undertaken to determine the nature of the interaction of n-octanohydroxamate with bastnaesite and rare earth oxides. Hydroxamate compounds of the rare earths, neodymium, erbium, dysprosium, gadolinium and holmium have been synthesised, and characterised by vibrational spectroscopy. Photoelectron spectra for neodymium hydroxamate were also determined. Neodymium oxide, bastnaesite (cerium) crystals (Pakistan) and Mountain Pass ore samples were treated with hydroxamate. Interaction was observed at the surface of both the rare earth oxides and the minerals. The research reported has established the feasibility of applying vibrational and photoelectron spectroscopy to study the interaction of hydroxamate collectors with rare earth minerals.

1. Introduction

The major ore source for light rare earth oxides (REO) is bastnaesite, a fluorocarbonate, that contains a mix of rare earth elements (REE) and yttrium. Monazite and similar REE phosphates are also important ores, and phosphosilicates form a significant ore source at Kvanefjeld. Other REO source ores include sorosilicate, allanite, and fluorapatite. Heavy REO ores are less abundant, and the main source is xenotime.

The approach used to concentrate bastnaesite minerals has been flotation with one of an n-octanohydroxamate, aromatic hydroxamate or fatty acid collector, often in conjunction with other separation techniques (Pavez et al., 1996; Sawaji et al., 1992; Zheng and Lin, 1994). Pradip and Fuerstenau investigated the flotation of bastnaesite from Mountain Pass using both fatty acid and alkyl hydroxamate collectors (Fuerstenau and Pradip, 1984; Pradip and Fuerstenau, 1983, 1991). They concluded that n-octanohydroxamate (OHA) was a more selective flotation reagent than the fatty acid collector. The investigation of hydroxamate flotation of REO minerals generally has been limited to n-octanohydroxamate (Pradip, 1988; Pavez et al., 1996; Perereia and Peres, 1997) and naphthalenic hydroxamate collectors (Xu et al., 2002; Ren et al., 1997, Cheng et al., 2007). Xu et al. (2002) used 1-hydroxy-2-naphthylhydroximic acid and obtained a 37% REO concentrate from an 11% feed with an 80% recovery. Ren et al. (1997) reported the use of a similar hydroxylated naphthalene hydroxamic acid with superior collection properties for the flotation of bastnaesite ore indicating there is scope for the development of more selective reagents.

Hydroxamates are the most commonly used flotation collectors, and they have been widely used to produce rare earth mineral concentrates in Chinese rare earth mineral plants

since the 1960s (Liu et al., 2006). These plants have produced around 2/3 of the world's rare earth production. Notwithstanding the fact that hydroxamate collectors are currently used productively for the concentration of some rare earth ores, there are yet to be developed rare earth ore-bodies that contain gangue minerals that might be expected to compete with the rare earth minerals for the hydroxamate collector. Accordingly, it is important to better understand the interaction of such collectors, not only with rare-earth host minerals, but also with the principal gangue minerals. An enhanced understanding requires direct surface and near-surface chemical characterisation, and the research reported here has been undertaken to assess the feasibility of applying X-ray photoelectron spectroscopy (XPS) and vibrational (Raman and infrared) spectroscopy for this purpose. Although XPS is an ex-situ, UHV-based technique, it has been applied successfully to numerous other mineral/collector systems. However, rare earth oxide minerals present specific problems for XPS characterisation, including the typical presence of several rare earth elements in the one host oxide, the complex nature of the photoelectron spectrum from each rare earth, and the potential interference by X-ray excited Auger electrons from O and F as well as the rare earth elements themselves. For near-surface characterisation, Raman spectroscopy has the advantage of both in-situ and ex-situ applicability as well as high spatial resolution, but beam damage to a collector such as hydroxamate when adsorbed on an oxide mineral is a potential problem with both techniques that requires examination.

For this assessment, the interaction of n-octanohydroxamate collector with bastnaesite has been investigated by vibrational and photoelectron spectroscopic techniques supported by scanning electron microscopy. The interaction of hydroxamate with neodymium oxide and a model gangue material, an ore sample that would typically contain rare earth minerals, was also studied. The nature of the rare earth/collector bonding in any multilayer coverage has been deduced from a spectroscopic characterisation of several bulk rare earth n-octanohydroxamates that were synthesised for this purpose.

4

2. Experimental

2.1. Materials

Solutions were prepared using Analytical Reagent (AR)-grade chemicals and doubly de-ionized (DDI) water. Neodymium oxide (Nd_2O_3), dysprosium oxide (Dy_2O_3), gadolinium oxide (Gd_2O_3), holmium oxide (Ho_2O_3) and erbium oxide (Er_2O_3) were purchased from Sigma-Aldrich. The n-octanohydroxamic acid (OHAH) was obtained by neutralising an alkaline (KOH) solution of potassium hydrogen n-octanohydroxamate (trade name AM28, supplied by Axis House) with sulfuric acid. The precipitated hydroxamic acid was filtered, washed with DDI water and dried in air. The sample was then recrystallised from methanol and dried in air before use. Bastnaesite crystals and bastnaesite ore, sourced from Pakistan and Mountain Pass in the USA, respectively, were purchased from BK Minerals (Brisbane, Australia).

2.2. Synthesis of the REE compounds with hydroxamate and interaction of hydroxamate with surfaces

REE hydroxamates were prepared after the method used by Feng and Fernando (1960) for preparing 4-hydroxybenzothiazole with rare earths. Rare earth oxides were dissolved in approximately 30 mL of 70% nitric acid with heating as required. The n-octanohydroxamic acid was dissolved in ethanol and then added to the rare earth nitrate solution at a ratio of 6:1. The reaction solvent consisted of 50/50 water and ethanol. Ammonia (25%) was added dropwise until the first permanent precipitate was observed, then 3-4 drops more of ammonia

solution was added. The pH was measured at this point. All the hydroxamate rare earth metal complexes (Nd, Er, Dy, Gd, and Ho) were synthesised in a similar manner.

Nd_2O_3 was chosen as the model compound to identify the interaction between oxides and hydroxamate. 0.5 g of Nd_2O_3 was added to 30 mL of potassium hydrogen n-octanohydroxamate (0.5 mmol dm^{-3} in 1:1 of ethanol: water (V/V)) at pH 13 (KOH) and conditioned for 52 h. The solid was collected by filtering, then washed 3 times with water, and dried under vacuum before further investigation.

The bastnaesite crystal was treated in potassium hydrogen n-octanohydroxamate (0.5 mmol dm^{-3} in 1:1 ethanol: water (V/V), pH 9.6) for 40 minutes before investigation. The bastnaesite ore was sliced using a diamond wafering saw lubricated with water and ground prior to use using silicon carbide paper to 400 grade to produce a flat sample for microscopic investigation, then the bastnaesite ore sample was located on the Raman microscope stage and a layer of the potassium hydrogen n-octanohydroxamate solution was contacted with the surface. Following the conditioning, the surface was washed three times with DDI water and dabbed to dry so as to retain the position of the sample on the microscope stage.

2.3. Scanning electron microscopy (SEM)

The bastnaesite ore sample from Mountain Pass was prepared by grinding and polished to 1 μm using a diamond lap. The mounted sample was etched for 20 s in 1 mol dm^{-3} HCl before washing, drying and coating with gold. Micrographs were collected using a JEOL JSM 6510LV with a 10–12 mm working distance, a spot size of 0.2 μm and a beam energy of 15 kV with secondary or back scattered electron detection.

2.4. Vibrational spectroscopy

The Raman spectra were recorded on a Renishaw inVia spectrometer using a 632.8 nm excitation from a HeNe laser. The scattered light was detected with a Peltier-cooled CCD detector with spectral resolution ~ 2 cm^{-1}. All the spectra were collected on a Renishaw InVia Raman spectrometer that has a rotary encoded grating stage and an internal two stage Peltier cooled (-70°C) CCD detector. Raman spectra were calibrated using the 520 cm^{-1} silicon band. Spectral manipulations such as baseline adjustment, smoothing and normalisation were performed with GRAMS32 software (Galactic Industries, Salem, NH, USA). Fourier transform infrared (FT-IR) spectra were undertaken on a Thermo Nicolet Nexus FT-IR spectrometer equipped with EverGlo IR source optics which provides a stabilised signal and 0.5 cm^{-1} resolution. The spectrometer had a DTGS detector with KBr window and Ge on KBr beamsplitter. FT-IR spectra were acquired in the range of 4000 - 100 cm^{-1}.

2.5. X-ray photoelectron spectroscopy

For mineral and ore specimens, most X-ray photoelectron spectra were collected from a surface of a single slice or crystal of area ranging from 1–8 mm^2 rather than particles of floatable size. The surface of a slice was abraded until relatively smooth to the unaided eye before conditioning in a saturated aqueous KH(n-octanohydroxamate)$_2$ solution at its unadjusted pH (~9.5), rinsing with water, and subsequent characterisation by XPS at ambient temperature. Crushed mineral particles can provide information that is more representative of the bulk than an abraded surface, and in the few cases such specimens were characterised, the fine particles were pressed into a freshly exposed surface of indium.

Specimens of microcrystalline compounds such as Nd hydroxamate were also prepared by pressing the powder into indium.

XPS data were obtained on an ESCALAB 250Xi spectrometer using monochromatised Al K$_\alpha$ X-rays focused to a spot size of 0.5 mm and an electron analyser pass energy of 20 eV for narrow range scans. Included in the binding energies employed for calibration were 83.96 eV for Au $4f_{7/2}$ of metallic gold and 932.6 eV for Cu $2p_{3/2}$ of Cu metal. The pressure in the analysis chamber was better than 5×10^{-9} mbar during spectral acquisition. Because of the poor electrical conductivity of the minerals and compounds investigated, photoelectron spectra had to be obtained while the specimen was under the influence of a low energy electron beam (4 V, 175 µA) from a charge-neutralisation flood gun. The observed binding energies, which were lower than the correct values because of over-compensation of charging to achieve minimum linewidth, were usually referenced to 285.0 eV for the hydrocarbon C $1s$ photoelectrons. The possibility of beam damage by the low energy electrons was monitored, and in order to minimise any damage, spectra were obtained as quickly as possible at the expense of signal-to-noise. The data were collected and processed under Thermo Scientific Avantage 4.58 and 4.54 software.

3. Results and discussion

3.1. X-ray photoelectron spectroscopy

3.1.1. Bulk Nd oxide

X-ray photoelectron spectra for bulk Nd oxide, nominally Nd_2O_3, were determined primarily for the purpose of checking the relative sensitivity factors used to convert peak

intensities to elemental composition in the XPS data processing software. It was expected that some Nd carbonate and hydroxide would be present near the surface of Nd oxide that had been exposed to the atmosphere, and indeed there was a component at 289.5 eV in the C $1s$ spectrum that could be attributed to carbonate. On the basis of the Nd $4d$ intensity (rather than the more intense but more surface-sensitive Nd $3d_{5/2}$), the composition of the surface layer was $Nd_{16}(CO_3)_9O_{26}$ (excluding H), which would be consistent with $[Nd_2O_3]_{1.5}[Nd_2(CO_3)_3]_3.[Nd(OH)_3]_7$. Such a composition would be in agreement with the O $1s$ spectrum, which was centred at 531.5 eV, without structure apart from a slight asymmetry, and without a component near 530 eV from oxide. However, because of the unknown surface concentration of Nd hydroxide, it was not possible to confirm the relative Nd $4d$ and O $1s$ sensitivity factors from the spectrum for the air-exposed oxide. As for all rare earth hydroxides, Nd hydroxide is a definite compound rather than a hydrous oxide.

Nd^{III} has the electronic configuration $4f^3 6s^0$, and when a $3d$ electron is photo-ejected from Nd^{III}, the final state has contributions primarily from the configurations $3d^9 4f^3$ and $3d^9 4f^4 \underline{L}$, where L is a ligand such as an O atom of an oxygen-containing group (when $\underline{L}$ would be $O^{-II} 2p^5$). The $3d^9 4f^3$ configuration predominates for Nd, therefore the higher binding energy component in the Nd $3d_{5/2}$ peak will be more intense than the lower binding energy component arising from the $3d^9 4f^4 \underline{L}$ configuration (Kotani and Ogasawara, 1992). The separation between these two components is about 3.5 eV for Nd^{III} oxide, and the two principal $3d$ peaks are separated by ~21.2 eV. Because of multiplet coupling, the shape of the Nd $3d_{3/2}$ and $3d_{5/2}$ peaks is different. Two of the O KLL Auger peaks are superimposed on the Nd $3d$ peaks, further complicating the already complicated spectral features and background. For the air-exposed Nd oxide, the main component of the Nd $3d_{5/2}$ peak was at 983.0 eV.

In general, for Nd^{III} $4d$ photoemission, multiplet coupling is much more important than for $3d$ because the exchange interaction between $4d$ and $4f$ states is much larger than

9

between $3d$ and $4f$ states. The $4d$ spin-orbit interaction is weaker than the $4d$–$4f$ exchange interaction, so the Nd $4d$ spectrum is not separated into $4d_{5/2}$ and $4d_{3/3}$ components. Each $4d$ spectrum, which typically has a width of more than 7 eV, contains a large number of components and cannot meaningfully be fitted with a small number of dominant contributions. The Nd $4d$ spectrum from the air-exposed Nd oxide was in accord with these expected features, and contained no resolved structure.

3.1.2. Bulk Nd hydroxamate

The expected elemental composition (excluding H) of Nd hydroxamate would be $Nd(C_8O_2N)_3$, in which case the atomic concentrations should be Nd 2.9 at%, C 70.6 at%, O 17.6 at% and N 8.8 at%. The quasi-surface atomic composition that is determined by XPS is expected to be slightly higher in C and O because of extraneous carbonaceous surface contamination. The measured elemental compositions of the three batches of Nd hydroxamate (synthesised from either potassium hydroxamate or hydroxamic acid) were broadly similar and close to $Nd_{2.6}(C_8O_2N)_3$ if minor C and O from surface contamination is ignored. Thus the prepared complexes might have had a slightly lower than expected Nd content, but as explained above, the accuracy of the Nd sensitivity factors used in the data analysis is unknown. No extraneous elements (including K) were detected, and the C $1s$ and O $1s$ spectra were similar to those for other n-octanohydroxamate complexes (Hope et al., 2011). The main component in the Nd $3d_{5/2}$ peak was at a binding energy of 982.4±0.2 eV, slightly lower than for air-exposed Nd oxide, but with a similar separation of ~3.5 eV between the major and minor components. While it was necessary to take the O KLL Auger peak at an equivalent binding energy of ~976 eV into account when determining the intensity of the Nd $3d_{5/2}$ peak, that Auger peak did not interfere with the determination of the main $3d_{5/2}$ binding energy.

The N 1s spectrum consisted of two partially-resolved components, and could be fitted with a more intense component at 400.9±0.1 eV, which can be assigned to protonated hydroxamate N, and the other at 398.9±0.1 eV, which probably would have arisen from deprotonated hydroxamate N, or N in a hydroxamate decomposition product. The component near 401 eV was much more intense in the N 1s spectrum determined at the outset than at the end of the spectral suite, therefore the lower binding energy component was almost certainly produced by damage caused by secondary electrons or the low energy electrons from the flood-gun. In fact the ~401 eV component accounted for more than 90% of the N 1s intensity at the outset, but less than 55% at the end, indicating that the Nd hydroxamate was particularly susceptible to beam damage. For the Nd hydroxamate prepared from hydroxamic acid, a minor N 1s component at 406.9 eV, which would have arisen from an impurity N/O species, was also observed. The intensity of this component became lower with increasing beam time, confirming that it did not arise from a beam degradation product.

It is interesting to note that the La n-octanohydroxamate prepared by Belkasem et al. (2010) was claimed to be $La(C_8H_{16}NO_2)_3 \cdot 6H_2O$. However, there was no evidence in the O 1s spectrum for water of crystallisation in the Nd hydroxamate prepared in this investigation.

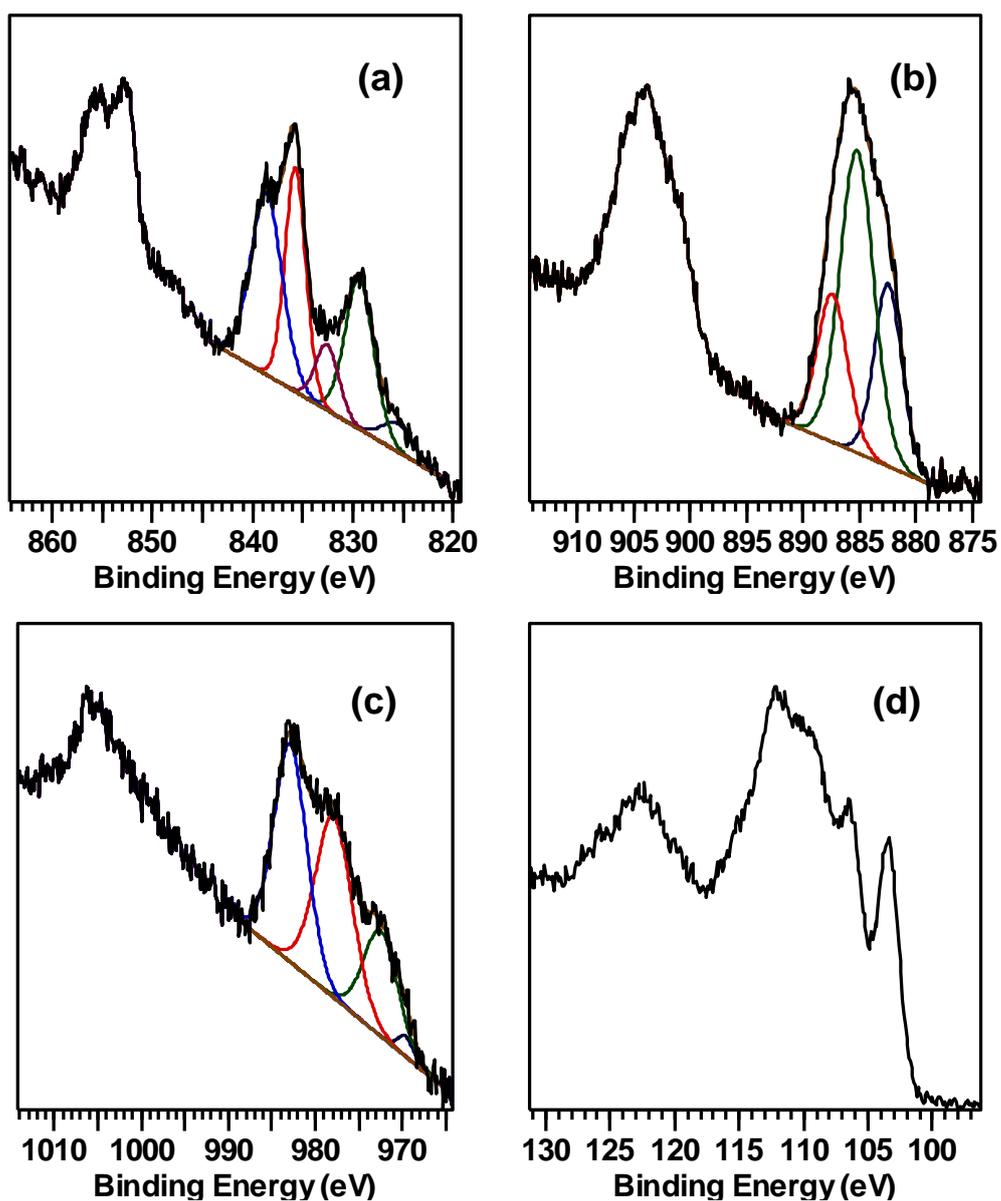3.1.3. Bastnaesite

The nominal composition of bastnaesite is $(Ce,La)FCO_3$, therefore even without other constituent elements such as Ca and Nd, interference of the La 3d spectrum from the F $KL_{2,3} L_{2,3}$ Auger peak at the equivalent binding energy of ~831 eV, and from a Ce $M_{4,5}N_{4,5}N_{4,5}$ Auger peak at an equivalent binding energy of ~832 eV, would be expected. As for the Nd 3d spectrum, the La and Ce 3d spectra are also intrinsically complex.

La^0 has a $4f^05d^16s^2$ electronic configuration, and La^{III} is $4f^05d^06s^0$. The La^{III} ground state is almost pure $4f^0$ configuration, but the $3d^94f^0$ and $3d^94f^1\underline{L}$ configurations are mixed very strongly in the final state resulting in two components (splitting ~2.7 eV) in each $3d$ peak with comparable intensities separated by ~17 eV. The slightly different structure (shape) of the two peaks is the result of multiplet coupling. Ce^0 has a $4f^26s^2$ electronic configuration, and Ce^{III} is $4f^16s^0$. The Ce^{III} $3d$ spectrum typically consists of two 'doublet' peaks (splitting ~4.3 eV) of different intensity separated by 18–19 eV. Mixing of the $3d^94f^1$ and $3d^94f^2\underline{L}$ configurations is slightly weaker than for La, so the lower binding energy peak of each doublet is slightly less intense.

The photoelectron spectra from crushed crystals and abraded surfaces of Pakistan bastnaesite indicated concentrations of Ce 2.1, Nd 1.7, La 0.8, F 4.1, Ca 2.9, and CO$_3$ 9.0 at%, suggesting that in addition to bastnaesite, Ca minerals such as Ca(Ce,La)$_2$(CO$_3$)$_3$F (parisite) and CaCO$_3$ (calcite) might be present. Ca $2p$ and Ce $3d$ XPS images of a 100 × 100 μm region on an abraded surface of bastnaesite revealed that the Ca was in a ~20 μm circular region within an 80 μm rectangular distribution of Ce that was relatively uniform at the μm level. The carbonate C $1s$ binding energy was 289.7 eV, and the O $1s$ binding energy of 531.6±0.1 eV was consistent with carbonate rather than oxide. No significant K, Mg or Ba was detected.

The La $3d$ spectrum (Fig. 1a) was broadly similar to that for La$_2$O$_3$ apart from interference by the F KL$_{2,3}$L$_{2,3}$ and Ce M$_{4,5}$N$_{4,5}$N$_{4,5}$ Auger peaks near 830 eV on the low binding energy side of the La $3d_{5/2}$ peak. The more intense low binding energy component of the La $3d_{5/2}$ peak was at 835.6±0.2 eV. The F $1s$ peak consisted of a single, symmetrical component of width ~1.45 eV at 684.8±0.2 eV, and the Ca $2p_{3/2}$ binding energy was 347.4±0.2 eV.

12

Fig. 1 Photoelectron spectra from an unconditioned bastnaesite surface: (a) La 3*d*; (b) Ce 3*d*; (c) Nd 3*d*; (d) Nd, Ce and La 4*d*.

By contrast, the Ce 3*d* spectrum (Fig. 1b) was more complex than that for Ce_2O_3 (Kotani and Ogasawara, 1992; Mullins et al., 1998), in that each 3*d* peak appeared to consist of 3 unresolved components, rather than two partially resolved ones. The separation of the outermost components was ~4.5 eV, which is not much larger than for Ce_2O_3, but the highest binding energy $3d_{5/2}$ component was near 887 eV, ~2 eV higher than that reported

13

for Ce^{III} oxide (Mullins et al., 1998). It is possible but unlikely that X-ray excited Auger peaks were superimposed on the Ce $3d$ spectrum. For example, any Ba present would have given rise to an $M_4N_{4,5}N_{4,5}$ peak at an equivalent binding energy near 889 eV and to a more intense $M_5N_{4,5}N_{4,5}$ peak near 902 eV, but a corresponding Ba $3d$ doublet at ~780 and 795 eV was barely discernible in the spectrum. It is more likely that the Ce $3d$ spectrum reflects the influence of the F in the structure of bastnaesite. In that structure, there are alternating $(RF)^{+II}$ and $(CO_3)^{-II}$ sheets such that each rare earth atom (R) has eight O and three F atoms as nearest neighbours (Hsu, 1992).

As expected, the Nd $3d$ peaks (Fig. 1c) were less intense than those from Nd oxide and therefore more affected by interference from the X-ray excited O KLL Auger peaks. Nevertheless, the binding energy (~982.9 eV) for the principal Nd $3d_{5/2}$ component obtained by fitting the $3d_{5/2}$ peak should have been free of interference.

The La, Ce and Nd $4d$ region of the photoelectron spectrum (Fig. 1d) was as expected given the observed $3d$ intensities for La, Ce and Nd. The La $4d$ spectrum was a doublet with the $4d_{5/2}$ peak near 103 eV, but because of dominant multiplet coupling, the Ce $4d$ spectrum near 111 eV contained no resolved structure, and the Nd $4d$ spectrum was a broad single peak near 123 eV. The $4d$ photoelectrons are less surface-sensitive than the $3d$, and consequently the $4d$ spectra are useful for comparison with the corresponding $3d$ spectra to obtain information from the two different analysis depths.

3.1.4. Bastnaesite conditioned in hydroxamate solution

Carbonate C (3.4 at%) remained evident in the C $1s$ spectrum from a surface of Pakistan bastnaesite that had been rinsed with water after conditioning in hydroxamate solution for 10 min, but the hydrocarbon C concentration was about 65 at%, indicating the presence of an adsorbate layer that was either thin if uniform, or in patches. The carbonate component

was relatively narrow (1.4 eV), whereas the hydrocarbon component consisted of several unresolved components. For this reason, binding energies for the conditioned bastnaesite spectra were referenced to the consistent set for carbonate C $1s$, F $1s$ and Ca $2p_{3/2}$ rather than to the hydrocarbon C $1s$ value. The retention of the F $1s$ peak, but with its intensity reduced to the same extent as the carbonate peak, supported the conclusion that the adsorbed layer must have been either thin or in patches.

The surface N concentration was 3.8 at%. The N $1s$ spectrum was asymmetric but contained no resolved structure and could be fitted with two components at 398.6 and 400.8 eV. Surprisingly, however, the lower binding energy component was the more intense even in the spectrum obtained at the outset. It is expected that most of the N would have been in hydroxamate adsorbed to La, Ce, Nd and Ca at the mineral surface, consequently it is not surprising that the N $1s$ and C $1s$ spectra were complex. It should be noted that the absence of K $2p$ peaks confirmed that no residual K from the collector remained at the surface. Notwithstanding the high initial intensity of the 398.6 eV component, it has been tentatively attributed to deprotonated hydroxamate N, but this assignment requires further investigation before it can be confirmed.

The La, Ce and Nd $3d$, La, Ce and Nd $4d$, and Ca $2p$ spectra were all similar to those from the unconditioned bastnaesite. That similarity would certainly be consistent with the chemisorption of hydroxamate to one or more of these elements. However, it would not necessarily be inconsistent with the adsorption of a thin (~monomolecular) layer of one or more of the molecular metal hydroxamates, as the metal $3d$ or $2p$ binding energies for the hydroxamates might not be markedly different from those for the corresponding carbonates or fluoro-carbonates. The presence of a significant concentration of one metal hydroxamate (in patches) at the conditioned surface can be ruled out, as since the relative intensities in the La, Ce and Nd $4d$ spectral region were essentially the same after conditioning as before, the more surface-sensitive $3d$ spectra should reveal a different relative intensity if one of

the metal hydroxamates had been formed preferentially. Furthermore, the possible formation of a significant concentration of La hydroxamate (in patches) can be eliminated, as the relative intensity of the F $KL_{2,3}L_{2,3}$ Auger peak near the La $3d$ spectrum was unchanged. Since the F would remain in the mineral substrate, but any La hydroxamate formed would be on top of the substrate and any chemisorbed hydroxamate, the La $3d$ intensity would increase relative to the F KLL peak if multilayer La hydroxamate were present at the surface. This means that a substantial adsorbed multilayer containing hydroxamates of La, Ce and Nd could not have been present. Together, these observations indicate that no more than one molecular layer of metal hydroxamates could have been retained at the rinsed bastnaesite surface.

3.1.5. Mountain Pass ore conditioned in hydroxamate

XPS characterisation of a piece of Mountain Pass ore containing essentially no rare earth elements showed that it consisted predominantly of minerals containing Ca, Mg and Ba, with minor Zr, Fe, Zn and Na. It is possible that there was a low concentration of Nd, but the F content was negligible, ruling out the presence of bastnaesite. An intense carbonate peak near 290 eV was observed in the C $1s$ spectrum, but there was no oxide component near 530 eV in the O $1s$ spectrum, indicating that the minerals were carbonates (or basic carbonates) rather than oxides. No K $2p$, nor Si $2p$ or $2s$ peaks were evident. The Ca $2p_{3/2}$ peak was at 347.5 eV, and the Ba $3d_{5/2}$ was at 780.55 eV.

Carbonate C (6 at%) remained well represented within the analysis depth at the surface of a slice of Mountain Pass ore conditioned for 25 min in hydroxamate solution, indicating that any adsorbate layer must have been thin. The presence of 4 at% N indicated that some adsorption of hydroxamate had occurred, possibly to Ca (5 at%) and/or to Ba (~1 at%). No Fe was detected at the conditioned surface. The N $1s$ spectrum determined at the outset

16

appeared to comprise at least two components, and could be fitted with a major component at 401 eV (75%) and a minor component at 399.4 eV (25%), whereas at the end of the spectral suite, the fitted components were at the same binding energies, but the major component only accounted for 60% of the total N 1s intensity. The increase in intensity of the lower binding energy component suggests that some deprotonation of adsorbed hydroxamate had occurred as a result of beam damage. The width (1.75 eV) of the two fitted components was sufficiently large to suggest that there might be a third component near 400.5 eV, and a better fit could be obtained on this basis, but the fit would not have been unique and in any case the component near 401 eV remained the most intense. A component between 400.0 and 400.6 eV might correspond to hydroxamate chemisorbed to Ca or Ba, while that near 401 eV would be consistent with fully protonated N in an adsorbed metal hydroxamate. Neither the Ca 2p nor Ba 3d spectrum was noticeably changed by the hydroxamate conditioning, but that would not necessarily preclude the presence of monolayer Ca or Ba hydroxamate. However, regardless of the adsorption sites or the identity of any adsorbed metal hydroxamate, the pertinent observation is the adsorption of hydroxamate at pH 9.5 at the surface of a gangue mineral that might potentially be an ore associate of bastnaesite. Of course in the presence of rare earth minerals, hydroxamate would be expected to preferentially adsorb on, or react with, the trivalent rare earth cations rather than the divalent alkaline earth cations.

3.2. Vibrational spectroscopy

3.2.1. Investigation of the REE hydroxamate compounds

Mineral flotation may be controlled by adsorption or surface compound formation, and it is important that the surface interaction characterisation be able to identify the nature of the

bonding between the flotation reagent and the target or gangue minerals. In particular, the closely related chemical properties of the lanthanide elements means that careful spectral characterisation of the lanthanide compounds is required if it is going to be feasible to observe individual lanthanide – hydroxamate interactions. REE hydroxamate compounds were synthesised in order to measure the spectral properties of the pure compounds.

Five REE complexes have been observed to precipitate at a pH that ranged from 4.2 to 5.5. Nd n-octanohydroxamate exhibited the highest precipitation pH of 5.5 while, as the atomic number of the REE increased: (Nd, Gd, Dy, Ho and Er), precipitation occurred at the decreasing pH values of 5.0, 4.6, 4.5 and 4.2. These results are consistent with those that Feng and Fernando (1960) found for rare earth complexes with 4-hydroxybenzothiazole. While the normal flotation conditions used for n-octanohydroxamate involve a substantially higher pH than the values at which precipitation of the REE hydroxamates were observed, it is likely that the pH used for flotation using AM28 will be an important separation variable.

Complexes were characterised using Raman and infrared spectroscopy. Fig. 2 presents the Raman spectra of Nd_2O_3, n-octanohydroxamic acid and Nd hydroxamate as well as the FT-IR of Nd hydroxamate.
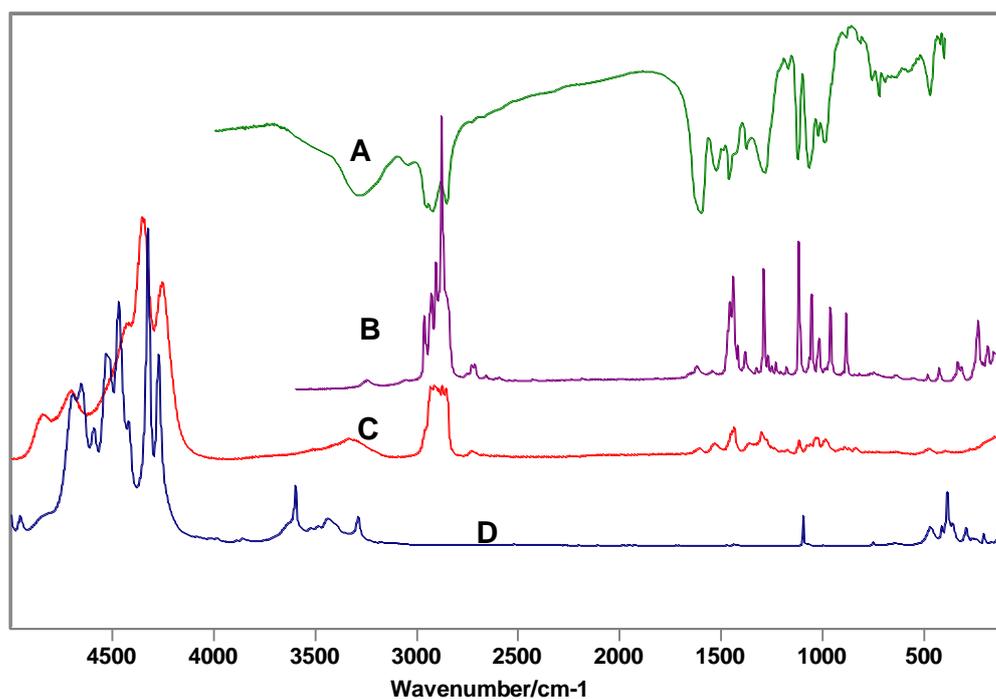
Fig. 2 A: FT-IR for Nd hydroxamate and Raman spectra of: B n-octanohydroxamic acid, C Nd hydroxamate and D Nd$_2$O$_3$.

The Raman band assignments for n-octanohydroxamic acid have been published (Hope et al., 2010). Fluorescence emissions from Nd can be observed in the oxide Raman spectrum. The fluorescence peaks observed for the oxide differ in intensity and energy from those for the hydroxamate. This is consistent with Nd electron energy level changes that result from the bonding of the Nd atom to oxygen of n-octanohydroxamate rather than the oxide.

The crystal structure of Fe^{III} tris acetohydroxamate has shown that the ligand coordination comprises three bidentate hydroxamate ligands in an octahedral configuration, with coordination occurring through the N-O and C=O oxygen atoms of the hydroxamate (Failes and Hambley, 2000; Alagha et al., 2011). This forms a five membered coordination ring. While the lanthanide cations may be able to coordinate a larger number of ligands, it is probable that all the lanthanides will be coordinated by 3 bidentate hydroxamate ligands. The vibrational spectra of the lanthanide complexes are expected to exhibit features that are

19

generated by this bonding. The spectral regions of particular interest are those that are derived from bonds directly involved with the coordination of the hydroxamate with the lanthanide cations. Table 1 shows the Raman and infrared assignments for C=O, C-N and N-O in the REE compounds and the ligand. As can be seen from Fig. 2 and Table 1, the Raman spectrum for the Nd hydroxamate exhibits a shift compared to that of the acid; in particular, C=O at 1622 cm^{-1} is shifted to lower wavenumber by 14 cm^{-1}. In contrast, C-N (1024 cm^{-1}) and N-O (970 cm^{-1}) are shifted to higher wavenumber by 4 and 15 cm^{-1} in the spectrum of Nd hydroxamate, respectively. The infrared spectrum also shows similar bonding shifts; in particular, C=O shifts from 1625 to 1603 cm^{-1} while N-O shifts from 1273 to 1288 cm^{-1} and C-N 970 to 996 cm^{-1}. This spectral change is consistent with bonding between Nd and n-octanohydroxamate through an N-O oxygen.

Table 1 Vibration spectra from REE hydroxamate, and n-octanohydroxamic acid.

| compound	Raman cm^{-1}			FT-IR cm^{-1}		
	$\nu_{C=O}$	ν_{C-N}	ν_{N-O}	$\nu_{C=O}$	ν_{C-N}	ν_{N-O}
Nd hydroxamate	1608	1028	988	1603	1288	996
Gd hydroxamate	1612	1031	991	1606	1297	997
Ho hydroxamate	1611	1041	994	1610	1306	998
Dy hydroxamate	1604	1032	998	1608	1299	998
Er hydroxamate	1611	1028	1000	1606	1288	997
n-octanohydroxamic acid	1662[a]	1024[a]	970[a]	1665[a]	1273[a]	970[a]

a Data sourced from Hope et al., 2010.
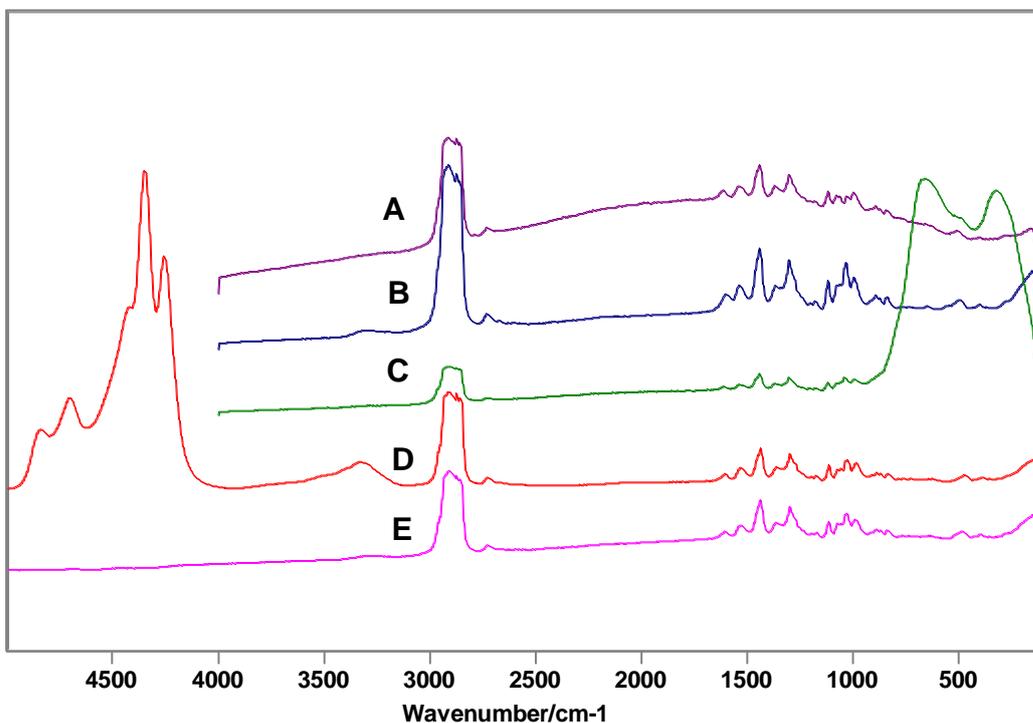
Fig. 3 Raman spectra from hydroxamates of Er, Dy, Ho, Nd and Gd, from top to bottom.

The REE comprise the lanthanides, scandium and yttrium. In the flotation system, these rare earth elements are expected to interact similarly with the collector, and consequently give rise to similar vibrational spectra. However, the spectra are also expected to be distinguishable due to differences in the atomic radius and valence electrons of the REE. For this reason, four more REE hydroxamate compounds were also investigated. Fig. 3 presents the Raman spectra for four REE hydroxamate compounds (Ho, Gd, Hy and Er) together with Nd hydroxamate. In Fig. 3 fluorescence emissions from holmium are apparent in the Raman spectrum below 900 cm^{-1}. Therefore, Ho and Nd are able to be identified through their fluorescent properties. For the expected bonding regions, the other four REE hydroxamate complexes (Ho, Gd, Hy and Er) exhibit similar Raman spectra to that observed for Nd hydroxamate. An average shift between 11 (1604-1612 cm^{-1}) and 9 (1028-1041 cm^{-1}) cm^{-1} is observed in the C=O and C-N bands whereas a shift to higher wavenumber of 24 cm^{-1} occurred for the N-O band (Table 1). These differences in the Raman band positions are

21

attributed to the small differences in the physical and chemical properties exhibited by the REE. It is feasible to distinguish between the REE compounds by careful comparison in the Raman bands.
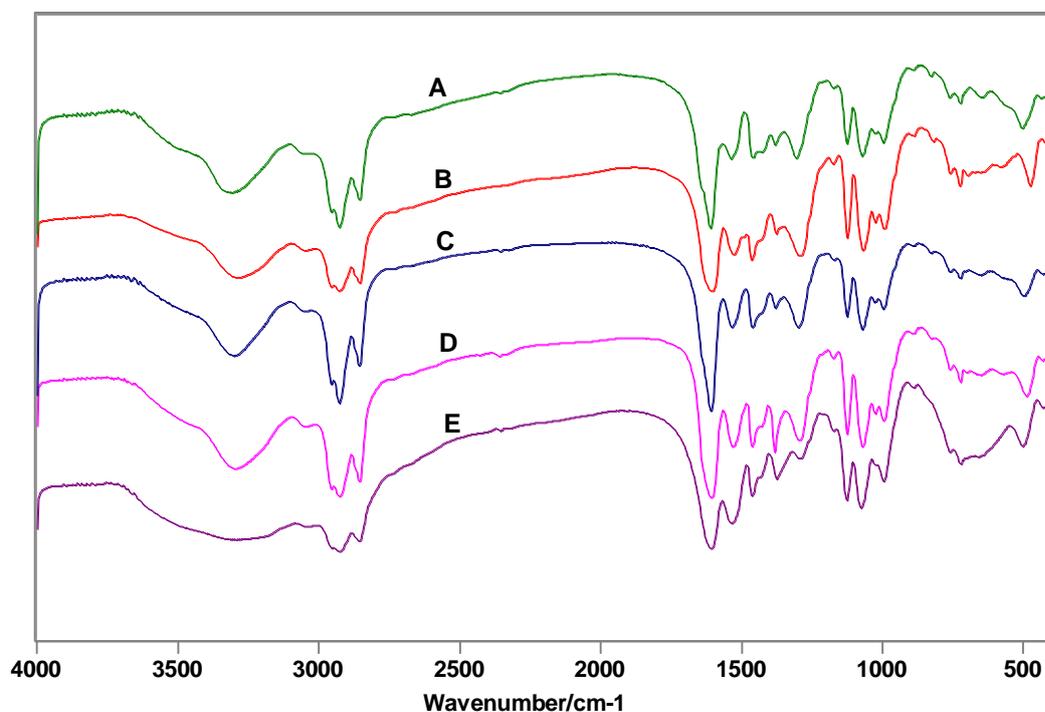

**Fig. 4** FT-IR spectra from hydroxamates of Ho, Nd, Dy, Gd and Er from top to bottom.

Infrared spectra were also determined for the five REE hydroxamate complexes synthesised and these show that a similarity of spectral properties is found in FT-IR as was exhibited in their Raman spectra (Fig. 4). The band for C=O shifted to lower wavenumber while the C-N and N-O shifted to higher wavenumber (Table 1). Huang et al. (1991) prepared 30 coordination compounds of the lanthanides and recorded their IR spectra. Their study showed a similar result in the bands of C=O (~ 1606 cm^{-1}) and N-O (997 cm^{-1}) for the five REE hydroxamate compounds prepared in this work. However, for the C-N band, the five compounds were reported slightly higher than 1300 cm^{-1} whereas in this work only holmium hydroxamate was observed above 1300 cm^{-1}.

3.2.2. Neodymium oxide, bastnaesite crystal and bastnaesite ore treated with n-octanohydroxamate

Nd_2O_3 was chosen as the model compound to investigate the interaction because neodymium n-octanohydroxamate is stable and we have the strong fluorescent emissions accessible for observation in a spectral region that does not overlap the Raman bands. Fig. 5 shows the Raman spectra of Nd_2O_3, $KH(OHA)_2$ and the $KH(OHA)_2$ treated Nd_2O_3. The treated sample exhibits all the expected spectral features from Nd_2O_3 including the fluorescence bands and the Raman bands, nevertheless, a 2 cm^{-1} of shift can be observed in the carbonate band (1096 cm^{-1}) and the fluorescence bands (Fig. 6-a, b, c). Additionally, from the treated sample in the region of 800-1700 cm^{-1}, bands that would be attributable to n-octanohydroxamic acid are absent while bands at 943 and 1636 cm^{-1} are evident.
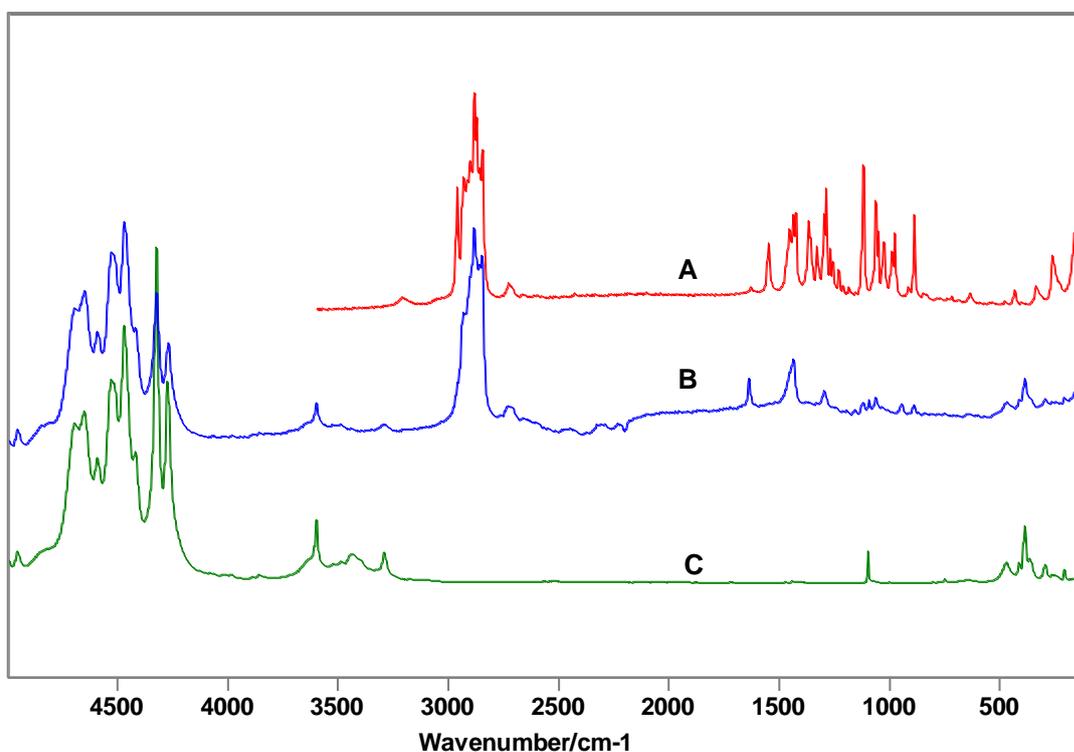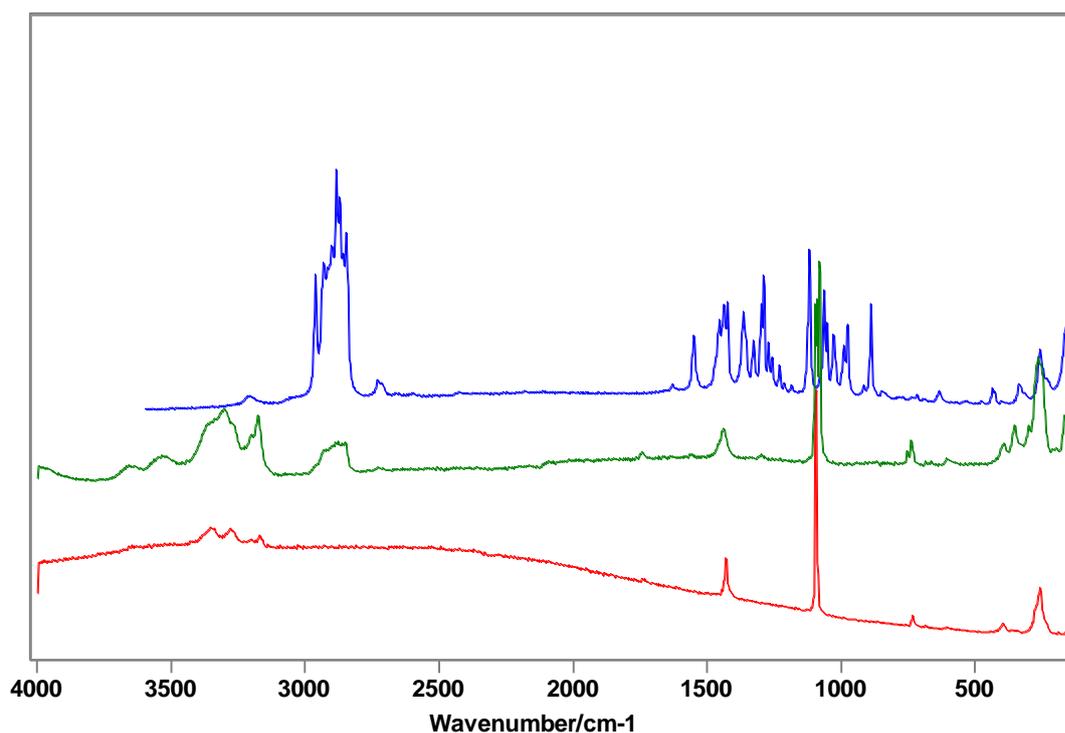

Fig. 5 Raman spectra for $KH(OHA)_2$ (A), $KH(OHA)_2$ treated Nd_2O_3 (B) and Nd_2O_3 (C).
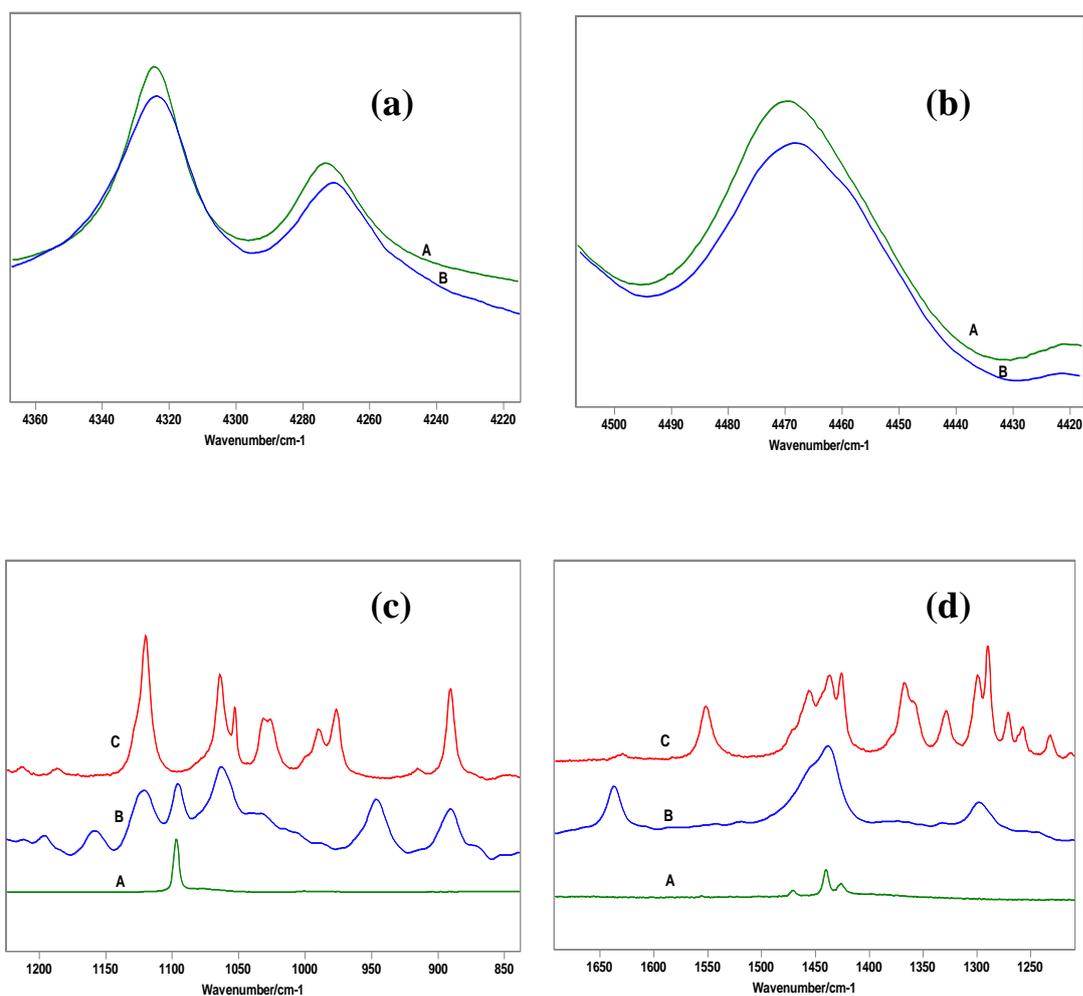
Raman spectra for Nd_2O_3 (A), $KH(OHA)_2$ treated Nd_2O_3 (B) and $KH(OHA)_2$ (C) in the range: (a) 4220-4360 cm^{-1}; (b) 4420-4500 cm^{-1}; (c) 850-1200 cm^{-1}; (d) 1250-1650 cm^{-1}.
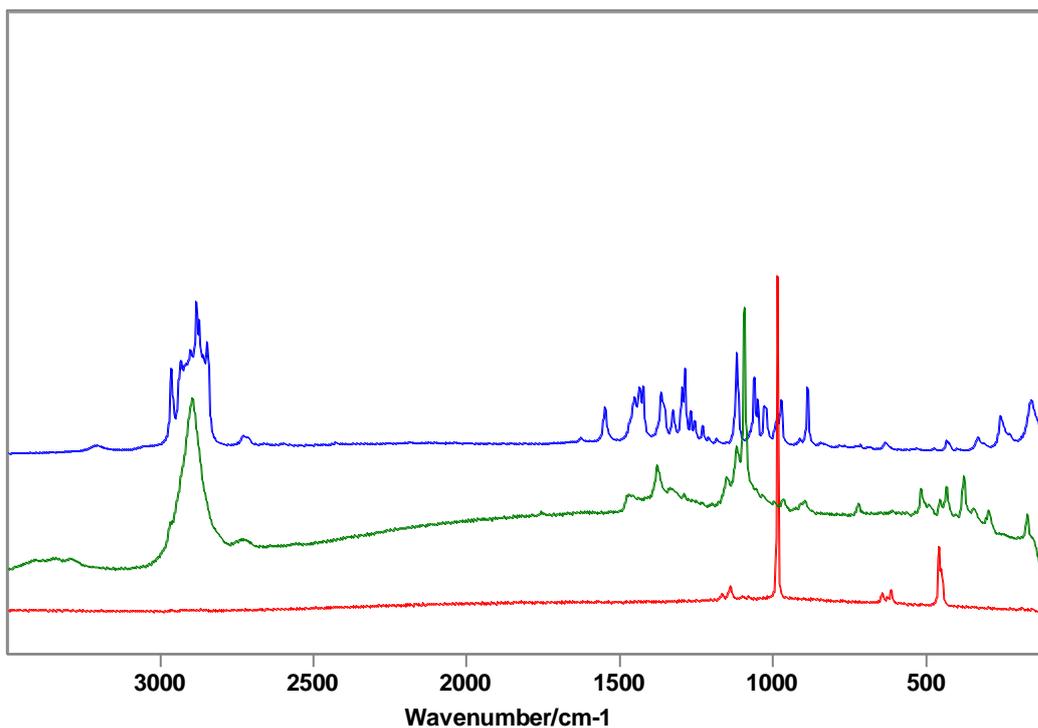
Fig. 7 Raman spectra for bastnaesite crystal, KH(OHA)$_2$ treated bastnaesite crystal and KH(OHA)$_2$ from bottom to top. The bastnaesite crystal sourced from Pakistan.

A bastnaesite crystal from Pakistan was investigated with vibrational spectroscopy. The collected bastnaesite data were consistent with those reported by Frost and Dickfos (2007) in which a single intense band at 1096 cm^{-1} assigned to $(CO_3)^{2-}$ symmetric stretching was presented, compared to the band at 1094 cm^{-1} that has been observed in this study. Fig. 7 shows the Raman spectrum for the KH(OHA)$_2$ treated bastnaesite crystal compared with the spectra from the crystal sample and KH(OHA)$_2$. Bands at 2846-2966 (broad) and 1437 cm^{-1} derived from KH(OHA)$_2$ are apparent in the spectrum of the treated crystal. In addition, a broad band at around 3300 cm^{-1} was observed which can be assigned to an N-H stretch. The spectrum is consistent with a multilayer of hydroxamate adsorbed on the surface of the mineral. This result might appear to be inconsistent with the XPS data because the conditioning treatment was different in the two cases.
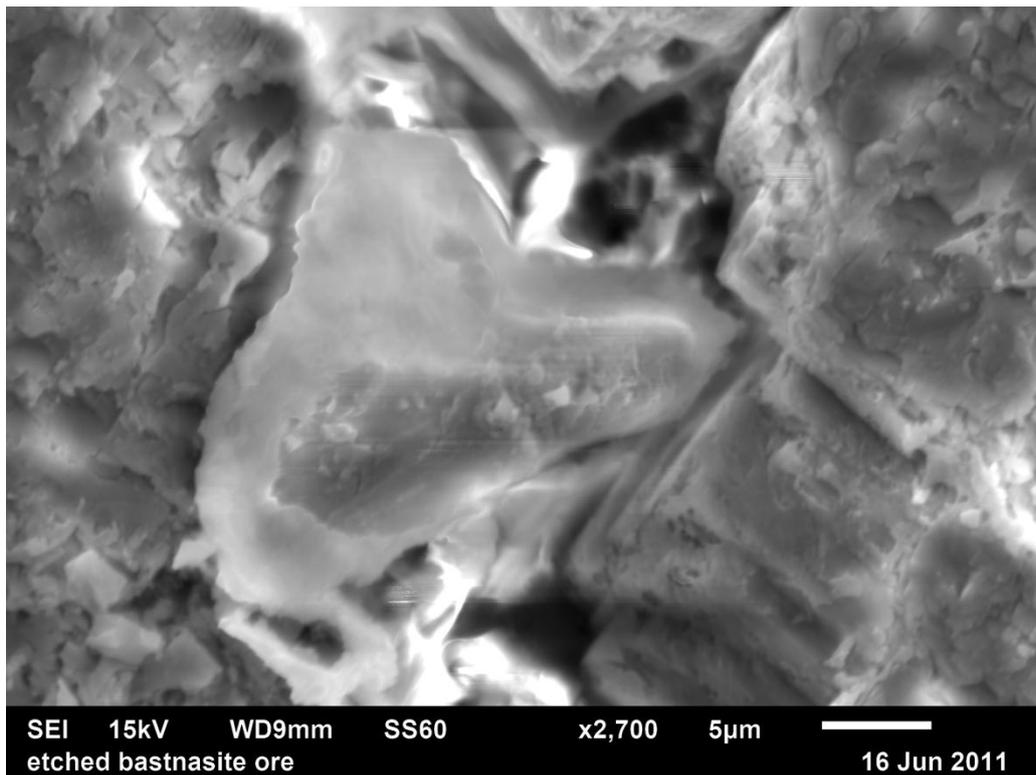
Fig. 8 Electron micrograph of a gold sputtered bastnaesite ore sample from Mountain Pass in USA (2,700 times magnification).

A specimen of bastnaesite ore from Mountain Pass was also investigated under the same conditions and was investigated by SEM before the OHA conditioning (Fig. 8). The SEM was conducted at 15 kV and with 2,700 times magnification. The etched surface displayed a 5 μm crystal showing that the surface was etched rapidly after being polished. However, the XPS investigation revealed that the specimen contained mainly Ca, Mg and Ba, and no REE were detected. Nevertheless, a single band at 2895 cm^{-1} presented in the $KH(OHA)_2$ treated bastnaesite ore; that band, which also featured in the spectrum from $KH(OHA)_2$ (Fig. 9), was consistent with hydroxamate compound formation on the ore surface. The result also suggests the flotation and separation of REE could be affected by the other metal elements in the same minerals, as the OHA might not only be bound to the REE components of the ore.

Fig. 9 Raman spectra for bastnaesite ore, KH(OHA)$_2$ treated bastnaesite ore and KH(OHA)$_2$ from bottom to top. The bastnaesite ore was sourced from Mountain Pass in USA.

4. Conclusions

Five REE hydroxamate compounds have been synthesized and investigated by vibrational spectroscopy. The spectra obtained were consistent with the bonding between REE and OHA. Differences in spectral bands were observed from the REE hydroxamate complexes, establishing the feasibility of distinguishing different REE in the complexes using vibrational spectroscopy. The hydroxamate conditioning of Nd$_2$O$_3$ also indicated multilayer adsorption on the surface. Surface chemical analysis of bastnaesite conditioned in hydroxamate solution has confirmed the feasibility of investigating bastnaesite flotation with XPS, Raman and FT-IR through the interaction of hydroxamate collectors with minerals containing rare earth elements. It was confirmed that the REE Auger peaks do interfere with the photoelectron spectra, but none of those peaks prevented the deduction of useful

information from the photoelectron spectra, and that some Auger peaks can be utilised in establishing the extent of collector coverage. Beam damage to the adsorbed collector was found to be a potential problem that could be largely obviated by the determination of photoelectron spectra from the most sensitive elements at the outset and again at the end of the spectral suite. In the absence of rare earth elements, adsorption of hydroxamate to potential gangue minerals was observed, but in the presence of rare earth elements, preferential adsorption to those elements would be expected.

Acknowledgements

References

Alagha, A., Parthasarathi, L., Gaynor, D., Muller-Bunz, H., Starikova, Z.A., Farkas, E., Brien, E.C.O., Gil, M.-J., Nolan, K.B., 2011, Metal complexes of cyclic hydroxamates. Synthesis and crystal structures of 3-hydroxy-2-methyl-3H-quinazolin-4-one (ChaH) and of its Fe (III), Co (II), Ni (II), Cu (II) and Zn (II) complexes. Inorganica Chimica Acta, 368, 58-66.

Belkasem, H.A., Benghuzi, S.A. and Desouky, O.A.M., 2010, Preparation and characterization of N-substituted octanohydroxamic acids metal complexes. Journal of Agricultural Chemistry and Biotechnology, Mansoura University, 12, 629–638.

Cheng, J., Hou, Y., Che, L., 2007, Flotation separation on rare earth minerals and gangues. Journal of Rare Earth, 25 (Spec.), 62-66.

Failes, T.W., Hambley, T.W., 2000, Crystal structures of tris (hydroxamate) complexes of iron (III). Australian Journal of Chemistry, 53, 879-881.

Feng, P.-K., Fernando, Q., 1960, Chelates of 4-hydroxybenzothiazole with the rare earths. Analytica Chimica Acta, 24 (1961), 548-554.

Frost, R.L., Dickfos, M.J., 2007, Raman spectroscopy of halogen containing carbonates. Journal of Raman Spectroscopy, 38 (11), 1516-1522.

Fuerstenau D.W., Pradip, 1984, Mineral flotation with hydroxamate collectors, in: M.J. Jones, R. Oblatt (Eds.), Reagents in the Minerals Industry, Institute of mining and metallurgy, London, 161-168.

Hope, G.A., Woods, R., Buckley, A.N., White, J.M., Mclean, J., 2010, Spectroscopic characterisation of n-octanohydroxamic acid and potassium hydrogen n-octanohydroxamate. Inorganica Chimica Acta, 363, 935-943.

Hsu, L.C., 1992, Synthesis and stability of bastnaesites in a part of the system (Ce, La)–F–H–C–O. Mineralogy and Petrology, 47, 87–101.

Huang, Y., Jiang, Q., Gu, Y., 1991, Preparation and properties of rare earths coodination compounds with benzohydroxamic acid and octahydroxamic acid (in Chinese). Journal of Inorganic Chemistry, 7 (3), 296-300.

Mullins, D.R., Overbury, S.H. and Huntley, D.R., 1998, Electron spectroscopy of single crystal and polycrystalline cerium oxide surfaces. Surface Science, 409, 307–319.

Kotani, A. and Ogasawara, H., 1992, Theory of core-level spectroscopy of rare-earth oxides. Journal of Electron Spectroscopy, 60, 257–299.

Liu, W., Wang, B., Dai, S., Ma, A., Wei, D., 2006, Current application and development prospect of hydroximic acid in flotation (in Chinese). Non-ferrous mining and metallurgy, 22 (4), 25-27.

Pavez, O., Brandao, P.R.G., Peres, A.E.C., 1996, Adsorption of oleate and octyl-hydroxamate on to rare-earths minerals. Minerals Engineering, 9 (3), 357-366.

Perereia C.A. and Peres, A.E.C., 1997, Flotation concentration of a xenotime pre-concentrate. Minerals Engineering., 10, 1291-1295.

Pradip, D.W. Fuerstenau, 1983, The adsorption of hydroxamate on semi-soluble minerals, part I: adsorption on barite, calcite and bastnasite. Colloids Surfaces, 8, 103-119.

Pradip, D.W. Fuerstenau, 1991, The role of inorganic and organic reagents in the flotation separation of rare-earth ores. International Journal of Mineral Processing, 32, 1-22.

Pradip, 1988, Applications of chelating agents in mineral processing. Minerals and Metallurgical Processing, 5, 80-89.

Ren, J., Lu, S., Song, S., Niu, J., 1997, A new collector for rare earth mineral flotation. Minerals Engineering, 10 (12), 1395-1404.

Sawaji, D., Yamashita, H., Maekawa, T., 1992, Flotation of rare-earth ions with octadecyliminobismethylenebisphosphonic acid. Analytical Sciences, 8, 247-250.

Xu, J., Xu, X., Wang, J., 2002, Synthesis of 1-hydroxy-2-naphthyl hydroximic acid and application to collecting rare earth minerals (in Chinese). Nonferrous Metals, 54 (3), 72-73.

Zheng, X.P., Lin, H.K., 1994, Mineralogy and flotation of rare-earth-bearing barium fluorophlogopite. Minerals Engineering, 7 (12), 1495-1503.